

Numerical Study on the Drag Reduction for a D-Shaped Bluff Body with Wavy Trailing Edge Structures

H. Yang, D. Luo[†] and T. Wang

School of Energy and Power Engineering, University of Shanghai for Science and Technology, Shanghai 200093, China

[†]Corresponding Author Email: luo.dahai@usst.edu.cn

ABSTRACT

The intricate and complex flow structures of three-dimensional unsteady incompressible turbulence surrounding bluff bodies have garnered considerable attention from numerous researchers. Using computational fluid dynamics (CFD) methodologies, the underlying mechanism by which a wavy trailing edge (TE) design for a D-shaped bluff body achieves drag reduction was explored. The wavy TE was in the form of a cosine wave with two design parameters: amplitude and wavelength. To ascertain optimal control parameters, we employed an improved delayed detached eddy simulation (IDDES) technique for a comprehensive parametric analysis, focusing on the amplitudes and wavelengths of the cosine wave. Furthermore, to gain a more holistic understanding of the factors influencing the design of wavy TE structures, we conducted parametric studies on three distinct groups of wavy structures. After identifying the optimal amplitude, wavelength, and wave type, we further investigated the control mechanism of the wavy structures in reducing the drag and mitigating lift fluctuations for Reynolds numbers in the range 3.6×10^5 – 3.6×10^6 . Present investigation revealed that compared with the original D-shaped bluff body, the wavy TE structures significantly reduced the average drag coefficient, with a maximum drag reduction of 60.2%. Moreover, it effectively curtailed the fluctuations in the lift coefficient. With careful parameter adjustments, the wavy TE significantly enhanced the characteristics of the flow field. This improvement was evident in the reduction in vortex scales, enhancement of instability characteristics in separated shear layers, and effective suppression of periodic vortex shedding.

Article History

Received June 4, 2024

Revised August 21, 2024

Accepted October 1, 2024

Available online January 1, 2025

Keywords:

D-shaped

Passive Control

Wavy Trailing Edge

Drag Reduction

Control Mechanism

1. INTRODUCTION

In recent years, drag reduction has garnered increasing attention, becoming not only a focal point in the industrial sector, but also a pivotal area of academic research (Marec, 2001). D-shaped bluff bodies serve as indispensable components in shipping, aviation, and automotive industries. The aerodynamic drag encountered by this component primarily originates from a pressure drag caused by flow separation in wake regions and vortex shedding. Numerous methods for bluff body flow control have been proposed to effectively reduce drag.

Currently, flow-control methods can be broadly categorized into two main types: active and passive. According to the current domestic and international research, the active control technology, which achieves drag reduction through external energy interventions, is a relatively mature approach. This approach includes

synthetic jets (Chen & Liao, 2021; Krishan et al., 2023), boundary-layer blowing/suction (Wang et al., 2024a), and plasma actuators (Xu et al., 2022). For instance, Kourta and Leclerc (2013) applied synthetic jet actuators for active control in their study on the Ahmed vehicle model. Their research findings indicated that under a Reynolds number of $Re=1.2 \times 10^6$, the maximum drag reduction reached 8.5%. This was primarily attributed to the interference effect of the synthetic jet, which shifted part of the vortex structures from the exterior to the interior of the boundary layer. This increased the energy within the boundary layer, enhanced its resistance to adverse pressure gradients, and consequently achieved significant drag reduction. Dai et al. (2024) used a traveling wave active control technique on the leading edge of a Naca0012 airfoil to investigate the effects of the dimensionless length and velocity of the traveling wave on the flow structure. The results showed that under optimal control parameters, the traveling wave can effectively suppress flow separation and significantly improve aerodynamic performance. In addition, Post and

Corke (2004) experimentally compared the flow control effects of two active control methods (plasma actuators and jets) on an NACA663-018 airfoil at high angles of attack. They discovered that the drag reduction effect was remarkable at an attack angle of 16° , with the drag coefficient decreasing by approximately 57.1% compared to that of an uncontrolled original airfoil. Active control methods are not only precise and efficient, but also highly adaptable, demonstrating excellent control effects in drag reduction. However, this approach also has drawbacks, including operational complexity and additional energy consumption.

By contrast, passive control methods do not require any external energy interference, making them structurally simple, cost-effective, and easy to implement. Among various passive control methods, wave structures have emerged as simple yet effective techniques. These structures have demonstrated significant achievements in enhancing the aerodynamic performance and optimizing the fluid flow dynamics, thereby attracting considerable attention from the scientific community. Fish and Battle (1995) found that fins of humpback whales possess a wave-like bulge structure with a sinusoidal distribution. Inspired by this, Chen et al. (2020) applied a sinusoidal corrugated structure to the leading edge of a blunt trailing-edge airfoil NACA0012. They conducted a parametric study on the effects of amplitudes and wavelengths on the aerodynamic performance at a Reynolds number of 4×10^5 . The results showed that both design parameters of the wavy airfoil were sensitive factors. At an attack angle of 10° , the lift-to-drag ratio of the wavy leading edge decreased by a maximum of 38.5% compared to that of the original airfoil. This is extremely helpful for mitigating stalling and improving the aerodynamic performance. Furthermore, this study found that as the amplitude increased, and the wavelength decreased, the aerodynamic performance weakened. To explore the reasons for this phenomenon, Zhang et al. (2013) conducted experiments to identify the key factors contributing to the loss of aerodynamic performance. The experimental results indicate that designing a corrugated modification for the airfoil makes it more susceptible to stalling, leading to earlier flow separation. The shedding of separated vortices is a crucial factor that causes lift reduction and aerodynamic performance degradation. Xing et al. (2023) investigated the noise reduction mechanism of a bionic wavy leading-edge on a blunt tail airfoil at $Re=400000$. Numerical results indicated that the wavy leading edge had a significant effect on reducing the trailing-edge noise of baseline airfoils, and the maximum sound pressure reduction was as high as 35 dB. Although extensive research has been conducted on the advantages and disadvantages of applying wavy structures to the leading edge, only few solutions address their shortcomings.

The research topics mentioned do not have a definitive solution at this stage; however, researchers still focus on exploring wavy structures as a crucial area of concern. The positioning of wavy structures at appropriate locations is vital for reducing drag and noise. Bearman and Tombazis (1993) and Tombazis and Bearman (1997) experimentally studied the three-dimensional characteristics of vortex shedding in a bluff body with a semielliptical shape by incorporating

wave structures into the trailing edge. The results indicated that the average pressure on the back increased with the amplitude of the introduced wavy structures, resulting in a significant reduction in drag. At a Reynolds number of 4×10^4 and an amplitude of 0.14, the maximum drag was reduced by 34% compared with the original bluff body. In addition, there are multiple modes of vortex shedding in the wavy TE, and there are significant differences in the vortex shedding frequency compared with the original bluff body, with the lowest frequency values obtained at the peak. This indicates that the wavy structures at the trailing edge can effectively suppress vortex shedding and change the structure of the flow field. Based on these results, Bearman and Owen (1998) designed wavy structures for the leading edge of a bluff. They found that even at some small amplitudes (0.06–0.09), the drag was significantly reduced by at least 30%. This further demonstrates that wavy structures can achieve significant drag reduction if they are positioned at the leading or trailing edges of the bluff body. Inspired by this, Darekar and Sherwin (2001) and others designed wave shapes on both the front and back surfaces of a square cylinder and explored the influence of the Reynolds number. Numerical simulation results showed that the double-wave structure maintained a drag reduction effect owing to the increase in base pressure. Simultaneously, its variation was also affected by the Reynolds number. When the Reynolds number was small ($Re=100$), the total drag was reduced by approximately 16%, and when the Reynolds number was increased to 500, the drag reduction significantly increased to 34%.

In addition to aerodynamics, wave structures designed for the tail section have been used to reduce noise in airfoil designs. Yang and Baeder (2016, 2019) were the first to apply a wavy structure to the trailing edge of blunt airfoils, and they achieved a wavy TE design by adjusting the local thickness. Their numerical results indicated that at an attack angle of 20° , which is in a stall condition, the aerodynamic performance was more prominent than that of the original airfoil when the tubercle aspect ratio was within an appropriate range. Based on optimal outcomes derived from the investigation of airfoil parametrization, they introduced these parameters to the entire blade and found that at higher wind speeds, the flow components integrated by the wavy TE became more significant, particularly as the separation at the blade root became stronger. The variation in the flow structures along a spanwise direction significantly contributed to noise reduction. However, this study did not focus on exploring noise reduction cases related to wavy structures on bluff bodies. Qi et al. (2024) optimized the blade without changing the blade stagger angle and explored the effect of a wavy trailing-edge structure with an amplitude of 2% of the chord length on noise. Their results showed that the wavy trailing edge promoted the conversion of layered vortices to comb vortices, resulting in an aerodynamic noise reduction of 2.6 dB. For more information, please refer to references Chen et al. (2022), Shi and Kollmann (2021), Smith and Klettner (2022).

A thorough analysis showed that the aforementioned studies primarily investigated the effects of amplitudes and wavelengths under low-Reynolds-number conditions when exploring the passive flow control of wavy structures. However, other potentially interfering factors

have not been adequately explored with regard to the drag-reduction mechanism of wavy structures. To more comprehensively analyze the flow control effects of wavy structures, this study focused on a typical D-shaped bluff body and implemented a wave modification design on its tail section. We parametrically studied the influence of amplitudes and wavelengths, as well as three different waveforms and their flow control effects under high Reynolds number conditions using the CFD method. Through an in-depth analysis of the obtained detailed flow field data, we aimed to gain a deeper understanding of the passive flow control mechanism of wavy TE modifications.

This study presented several simulation challenges. The wavelike design formed by self-propagating waves introduced unavoidable geometric perturbations in the initial model. These perturbations were closely related to the scaling effect of the boundary layer of the model. Therefore, the plotting of a 3D model requires a deeper understanding of these values. In addition, checking the scaling effects of the undistorted and distorted models is an extremely important part of this study.

2. GEOMETRIC DESCRIPTION AND NUMERICAL METHODS

2.1 Geometric Model

This study selected a D-shaped bluff body model, which consisted of a semicircular front section and rectangular prism at the back. The total length (L), span length (S), and main body height ($D=2d$) were 48 mm ($1.92D$), 75 mm ($3D$), and 25 mm, respectively. The front

end of the tail was set as the origin of the coordinate system. Figure 1 shows the original geometric model alongside the three-dimensional geometric model, featuring a cosine variation along the spanwise direction at the tail. In this study, the parameters for the design of the wavy structures at the tail were the wave amplitude and wavelength. The geometric parameter expression along the spanwise direction is formulated as follows:

$$D_z = D_{mean} + 2a \cos\left(\frac{2\pi z}{W}\right), \quad (1)$$

where D_z denotes the local height of the D-shaped bluff body in the spanwise direction, and a and W represent the amplitude and wavelength of the wave surface, respectively. D is the bluff height, and D_{mean} is the arithmetic mean of the local maximum and minimum thicknesses, denoted as D_{max} and D_{min} , respectively.

Three distinct geometric models of the wavy TE are presented in Fig. 1, and all these models have body heights and spanwise lengths identical to those of the original D-shaped model. To analyze the wave patterns, three rectangular slices were defined based on the numerical values of the wave amplitudes at different positions. These slices corresponded to the cross-sectional planes where the peaks, troughs, and middle of the wave structures were situated.

2.2 Computational Grids and Boundary Condition

Computational domains and boundary conditions are illustrated in Fig. 2. The inlet and outlet boundary conditions were set as the velocity inlet and pressure

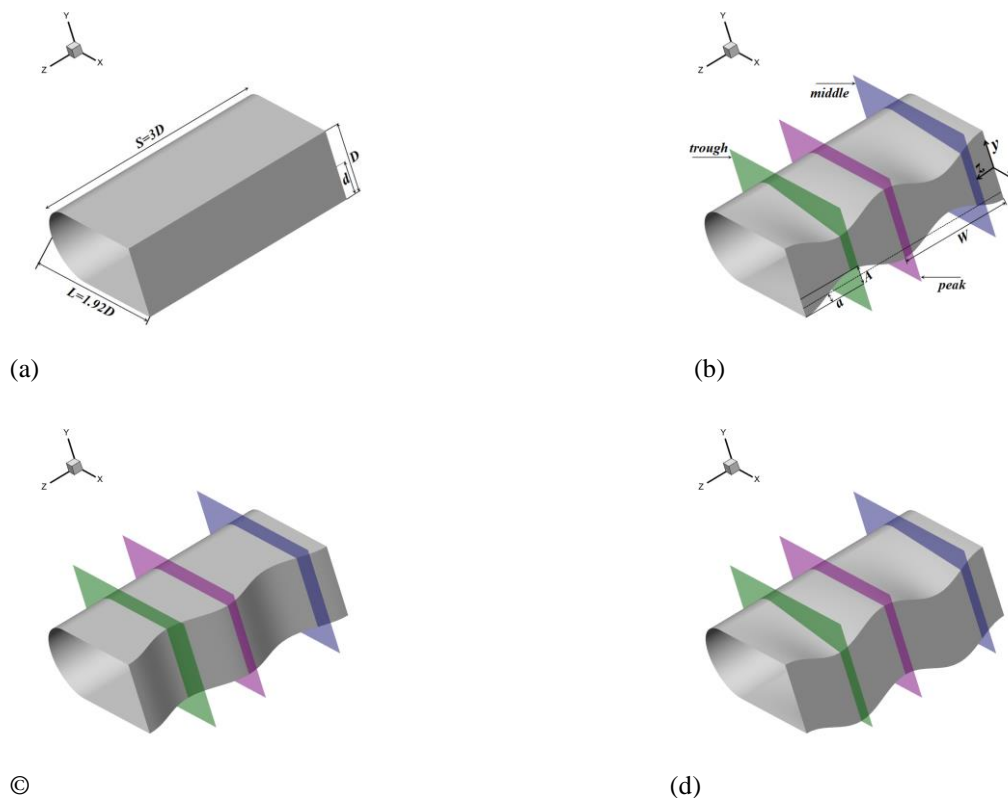


Fig. 1 Schematic diagram of the calculation models: (a) D-shaped, (b) wavy TE-I, (c) wavy TE-II, (d) wavy TE-III

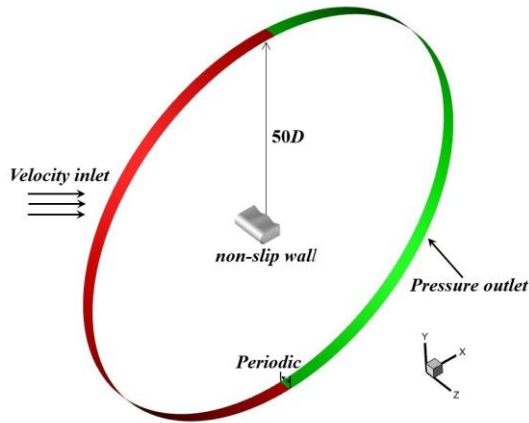


Fig. 2 Computation domain and boundary conditions

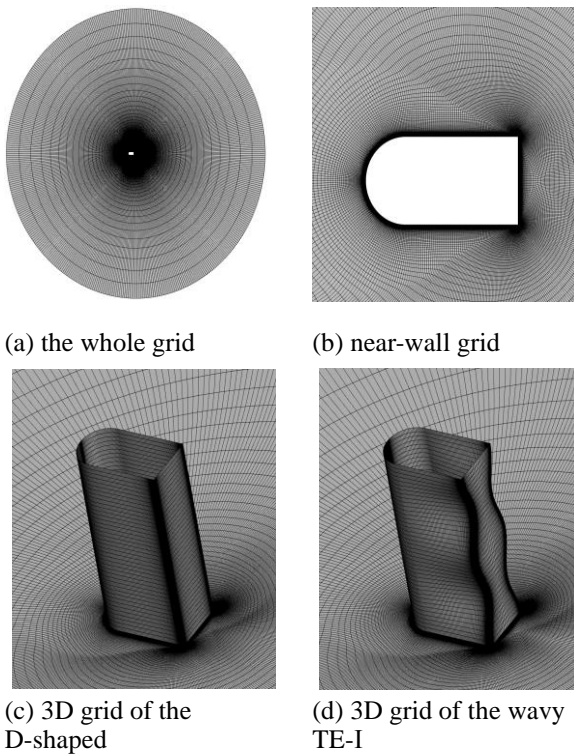


Fig. 3 Grid distributions of the D-shaped and wavy TE-I

outlet, respectively, and the main body wall was designated to have an adiabatic no-slip condition. In the three-dimensional CFD simulations of the wavy trailing edge (TE), periodic boundary conditions were applied along the spanwise direction. The computational grid is shown in Fig. 3. The overall structure adopted an O-shaped topology with structured grids refined near the wall and wake regions. The dimensions of the benchmark grid (circumferential \times normal) was 443×134 , with 59,362 surface grid cells. The length of the spanwise computational domain was $S=3D$, with 41 uniformly distributed grid nodes, which yielded a total grid count of approximately 2,417,360 cells. The height of the first grid layer normal to the main body wall was set to 5×10^{-6} to ensure y^+ values were less than 1.0.

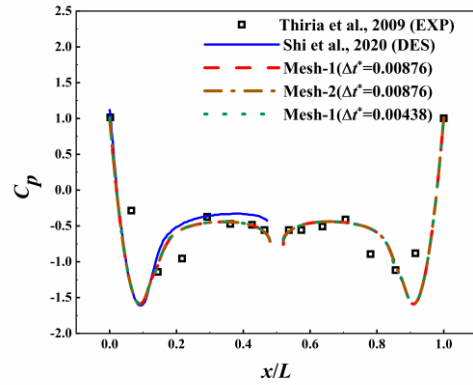


Fig. 4 Distribution of the pressure coefficient around the main bluff body

2.3 Numerical Validation

In this study, the commercial software ANSYS Fluent was employed, and the flow field data from three-dimensional steady incompressible RANS calculations was used as the initial field. A pressure-based solver was selected by employing the classic SIMPLE algorithm adopted for pressure-velocity coupling. A second-order scheme was applied for both pressure and temporal discretization. The working fluid was air, with a density and dynamic viscosity (μ) of 1.225 kg/m^3 and $1.7894 \times 10^{-5} \text{ Pa}\cdot\text{s}$, respectively. The aerodynamic force calculations for the D-shaped bluff body are performed using the IDDES method, which is based on the $k-\omega$ SST two-equation mode.

Figure 4 illustrates the effects of different grid densities and dimensionless time-step sizes on the pressure distribution on the upper and lower surfaces of the D-shaped model (all calculations were performed using IDDES). Two sets of grids with volumes of 2.5×10^6 and 4.7×10^6 were utilized. At a constant non-dimensional time, the outcomes obtained from the two grid sets exhibited a consistent trend and were closely aligned with the DES model adopted by Shi et al. (2020). Furthermore, our IDDES computational model exhibited closer alignment with the experimental data (Thiria et al., 2009). When the dimensionless time-step size $\Delta t^* = (\Delta t U_0)/D$ was reduced to 0.0063, the surface pressure distribution exhibited no change, indicating that the computation results at this point were independent of the time scale. Therefore, subsequent calculations in this paper adopt a dimensionless time of $\Delta t^* = 0.0126$, corresponding to a physical time-step of $\Delta t = 1.5 \times 10^{-5} \text{ s}$. One vortex shedding cycle covers roughly 400 time-steps to guarantee a fully established flow.

Figure 5 compares the velocity distribution obtained using the current IDDES method with experimental measurements. The results obtained from a finer grid, as compared to a coarser grid set, exhibited a closer agreement with the experimental data near the tail station. Despite the minimal differences in the numerical predictions of the two grid sets, both demonstrated good alignment with the experimental data. Considering both the computational accuracy and cost, Mesh-1 ($\Delta t^* = 0.0126$) has been chosen as the benchmark grid for this study.

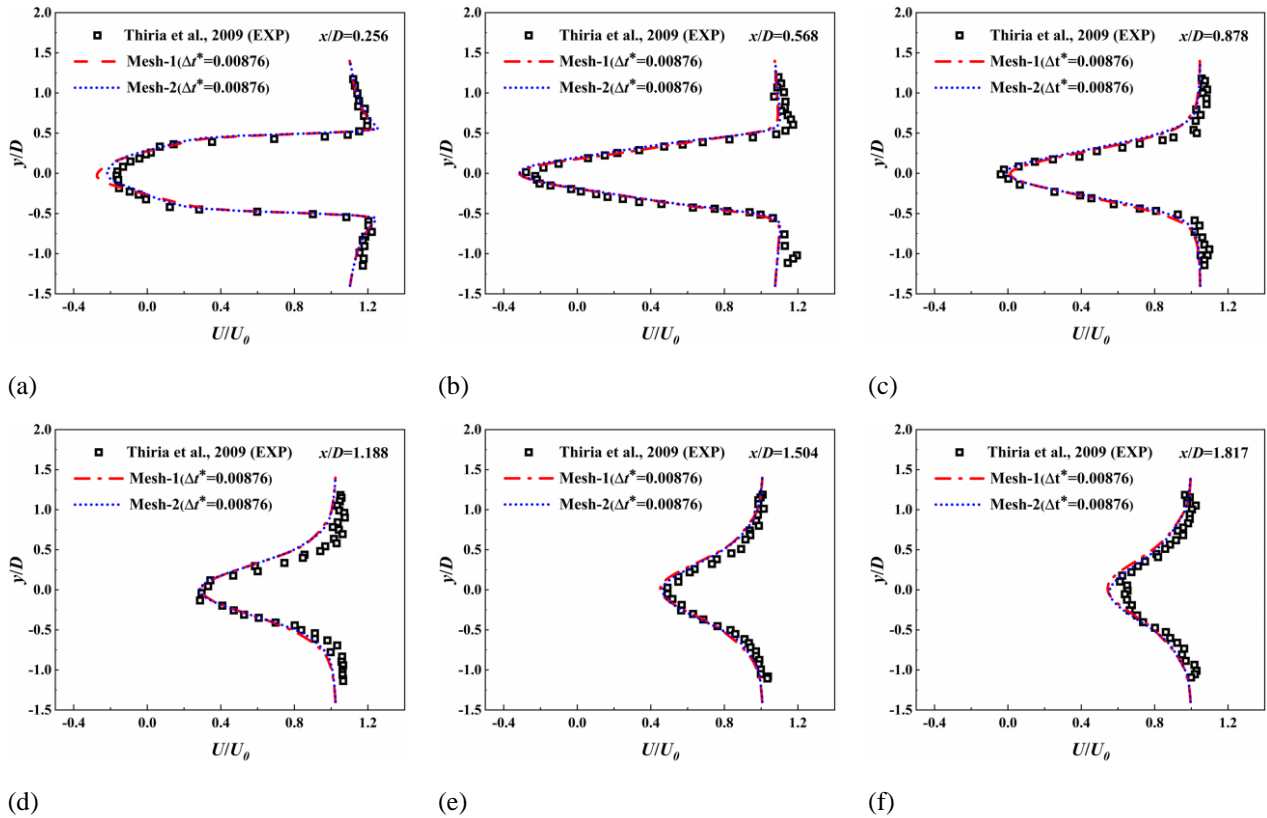


Fig. 5 Time-averaged flow velocity distribution at different stations

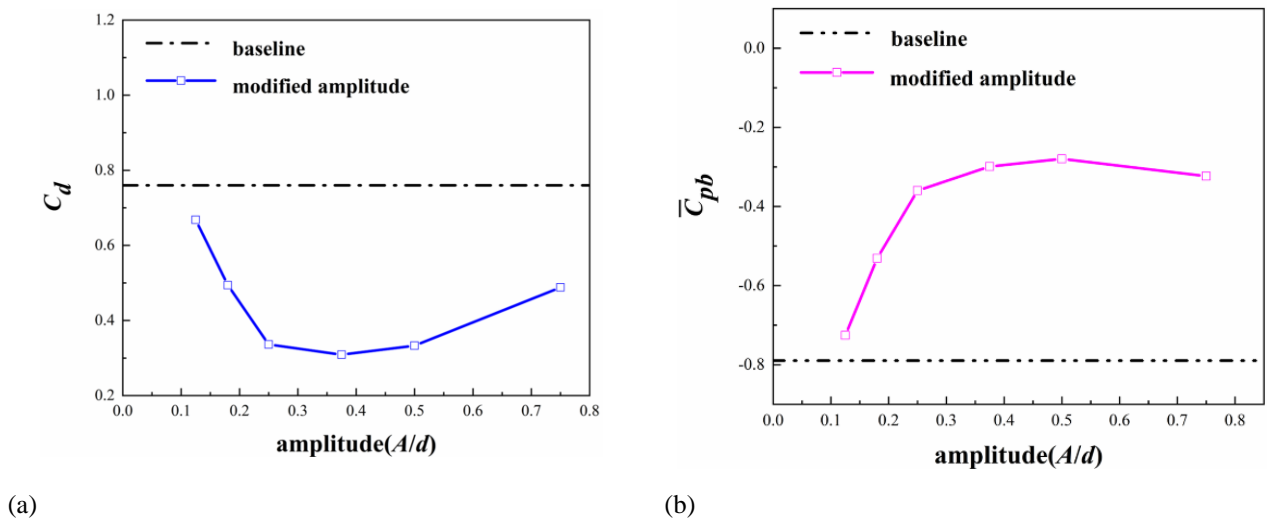


Fig. 6 Comparison of drag coefficient (a) and base pressure coefficient (b) at varying amplitudes

3. RESULTS AND DISCUSSION

3.1 Effect of Amplitude and Wavelength

Based on the wavy TE structures, the wavelength and wave amplitude are two crucial geometric parameters. Different types of wavy TE and incoming flow Reynolds numbers are also factors worthy of further exploration and will be discussed later. In this paper, a parametric study of the wavy TE-I (a specific configuration of the wavy TE) perpendicular to the

spanwise direction is conducted, considering an incoming flow Reynolds number of $Re = 3.6 \times 10^4$. The wave amplitude was studied within an A/d range of 0.18–0.75. After determining the optimal wave amplitude for drag reduction, the wavelength variation ($W/D = 0.75-3$) was explored while keeping the wave amplitude (A) constant, to investigate its impact on the aerodynamic performance and flow structures of the modified shape.

As shown in Figs. 6 and 7, the application of wavy structures to the tail of the model significantly reduced

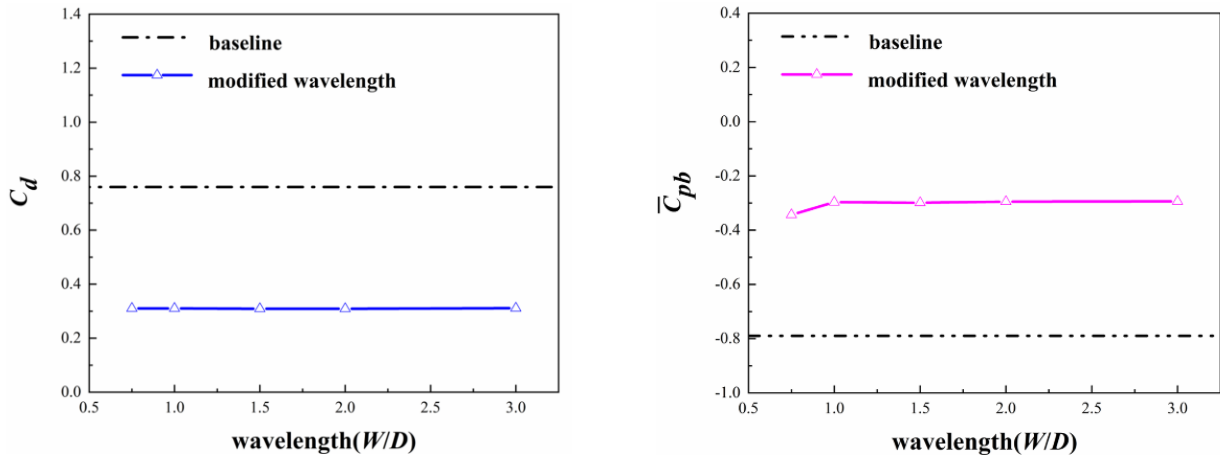


Fig. 7 Comparison of drag coefficient (a) and base pressure coefficient (b) at varying wavelengths

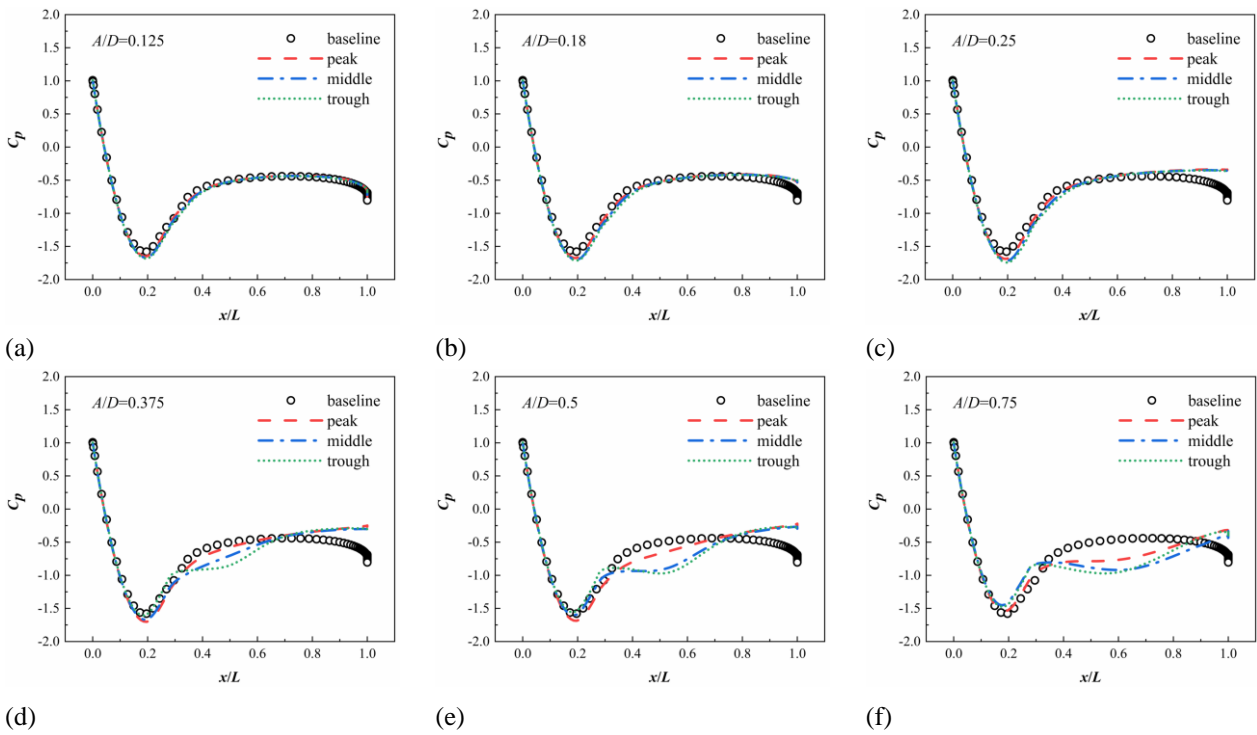


Fig. 8 Comparison of the surface pressure coefficient on D-shaped and wavy TE-I

its aerodynamic drag. At a constant wavelength at $W/D=1.5$, further drag reduction was attained by adjusting the wave amplitudes. Specifically, within an A/d range of 0.125–0.375, there was a noticeable upward trend in the drag reduction effect as the amplitudes increased gradually. Compared to the original model, the wavy TE achieved a drag reduction of approximately 59.3 %. Additionally, an increase in average base pressure coefficient to -0.30 along the spanwise direction significantly contributed to the drag reduction. However, when the wave amplitude continued to increase to $A/d=0.75$, the base pressure stabilized; however, the drag increased slightly but remained consistently lower than the drag level of the original model.

To further explore the drag reduction potential of wavy structures, we conducted a parametric study by varying the wave amplitudes and identified the optimal

wave amplitude for maximizing drag reduction. Subsequently, we investigated whether changing the wavelength could further enhance the drag-reduction effect. However, experimental results indicated that within the range of a single wavelength ($W/D=0.75-3$), variations in wavelengths have almost no impact on drag changes. Thus, we conclude that wavelength, one of the parameters in this study, is not a sensitive factor in exploring drag reduction with a wavy TE.

Figure 8 compares the time-averaged pressure coefficients on the upper surface of the variable amplitudes of wavy TE-I. In the leading region far away from the tail, the time-averaged pressure coefficient distribution and position of its minimum value within a small-amplitude range ($A/d=0.125-0.25$) were similar to those of the original D-shaped surface. However, the numerical values were slightly lower. As the amplitude

progressively increased, the pressure coefficient exhibited an upward trend. Notably, at the maximum amplitude of $A/d=0.75$, the pressure coefficient surpassed the baseline value at all three cross sections near the separation point. This increase was attributed to the influence of the wavy TE structures on the separated shear layer. In the region near the wavy structures, the time-averaged pressure coefficients for the three segments under a single wave amplitude were significantly higher than the baseline value, reaching a maximum at the tail. Furthermore, this difference increased as the amplitude increased. Additionally, the pressure coefficient at the peak was always higher than those at the trough and middle planes, particularly in the sections adjacent to the central area.

Figure 9 shows a comparison of the time-averaged velocity streamlines of the D-shaped prototype and its modified tail wavy design with different wave amplitudes. As shown in the figure, the shear layer of the original model remained relatively stable, with a pair of quasi-symmetric vortex structures present behind the trailing edge, showing no significant variation along the spanwise direction. However, by employing the IDDES method for the simulation, it became evident that the recirculation region at the tail of the body experienced a significant expansion as the amplitudes of the cosine waveform progressively escalated.

When the amplitude was $A/d=0.25$, at the peak plane, the quasi-symmetric vortex structure became more elongated compared to the unmodified trailing-edge vortex, and the recirculation region shrunk, leading to a significant reduction in drag. As the amplitude further increased to $A/d=0.375$ and beyond, the separation shear layer of the wavy structures became disordered, resulting in significant changes in the flow separation on all cross sections. At the peak, the wake region of the body extended, and the turbulence core shifted downstream; however, a pair of vortex structures was maintained. Similar to the flow separation phenomenon observed in the peak section, the vortex in the middle section moved downstream, but its size decreased sharply. In particular, at a wave amplitude of $A/d=0.5$, no flow separation occurred in the wake region. In the figure, compared with the original D-shaped cross-section at $Z/3D=0.75$, the original vortex pair in the trough wake region of the large wave amplitude range ($A/d=0.375-0.75$) moved upstream and attached uniformly to both the upper and lower wall surfaces. This led to changes in the location of the turbulence core and a reduction in the scales of the vortices.

Overall, the wavy modifications of the tail design can effectively suppress vortex shedding and enhance the flow field dynamics, especially under the effect of larger wave amplitudes, where the interference effect on the flow structures is more significant.

To significantly understand the influence of tail modifications on primary flow structures, three-dimensional transient flow configurations inherent in the original D-shaped and wavy TE were simultaneously exhibited upon computational convergence. The three-dimensional instantaneous flow field structures of the D-shaped and wavy TE-I configurations, visualized using the Q -criterion (non-dimensional with $Q=0.5$), are presented in Fig. 10.

The observations revealed significant differences between the spanwise flow structures of the modified and original D-shaped designs. More precisely, as the wave amplitude increased, interference at the separation shear layer near the head became more intense. Compared to the original model, which maintained a stable attached flow, the separation position on the modified surfaces advanced significantly. A comparative analysis showed that the shear layer on the wavy surface of the tail experienced instability in the downstream region. When the wave amplitudes reached $A/d=0.25$ or above, the shear layer became unstable, and large vortices gradually transformed into smaller-scale vortex structures and developed downstream.

The modified design of the wavy TE significantly affected the flow characteristics. Specifically, the vortex located at the trough of the wavy TE partially hindered the shedding of the separation vortex, resulting in a denser concentrated distribution of vortex structures in the main stream fluid, which predominantly accumulated in the trough region. Furthermore, the vortex scales of the wavy TE were substantially reduced, and periodic vortex shedding in the flow field was suppressed. This alteration in the flow characteristics increased the spanwise base pressure, a crucial factor for achieving excellent drag reduction.

3.2 Effect of Types of Wavy Structures

Drawing upon prior investigations on wavy TE-I, characterized by a cosine wave shape with its mirror aligned perpendicular to the spanwise direction, this study further explored two distinct variations of cosine wave types. To ensure the predictive accuracy of the computational simulation method, numerical simulations were performed on horizontal (wavy TE-II) and same-phase (wavy TE-III) configurations. Then, the drag changes corresponding to different wave amplitudes were calculated.

As shown in Fig. 11, all wavy modifications had a significant effect on reducing the overall drag. In the latter two passive control designs with wavy structures, when the wave amplitudes were small, the change in drag was minimal and approached the drag characteristics of the original model. For the wavy TE-II, when the amplitudes increased to $A/d=0.25$, the drag reduced, with a 5.92% reduction in the drag coefficient (0.715). As the wave amplitudes increased, the flow structures became more complex, and the drag coefficient experienced a gradual upward trend within a certain range. However, the values within this range were always smaller than the drag coefficient of the original model, ensuring that the wavy TE-II improved the overall aerodynamic performance. When the wave amplitudes increased to $A/d=0.75$, the drag coefficient suddenly decreased by 15.92%, achieving an optimal drag reduction effect. For the wavy TE-III model, modifying the wave amplitudes resulted in changes to the drag coefficient, resembling the numerical simulations of the wavy TE-I. When the wave amplitudes reached $A/d=0.12$ or higher, the drag coefficients first decreased to a minimum value of 0.489 and then exhibited a clear upward trend as the wave amplitudes continued to increase. Notably, the optimum wave amplitude value for drag reduction ($A/d=0.5$) exhibited a delay due to the diverse degrees of interference induced by distinct wavy

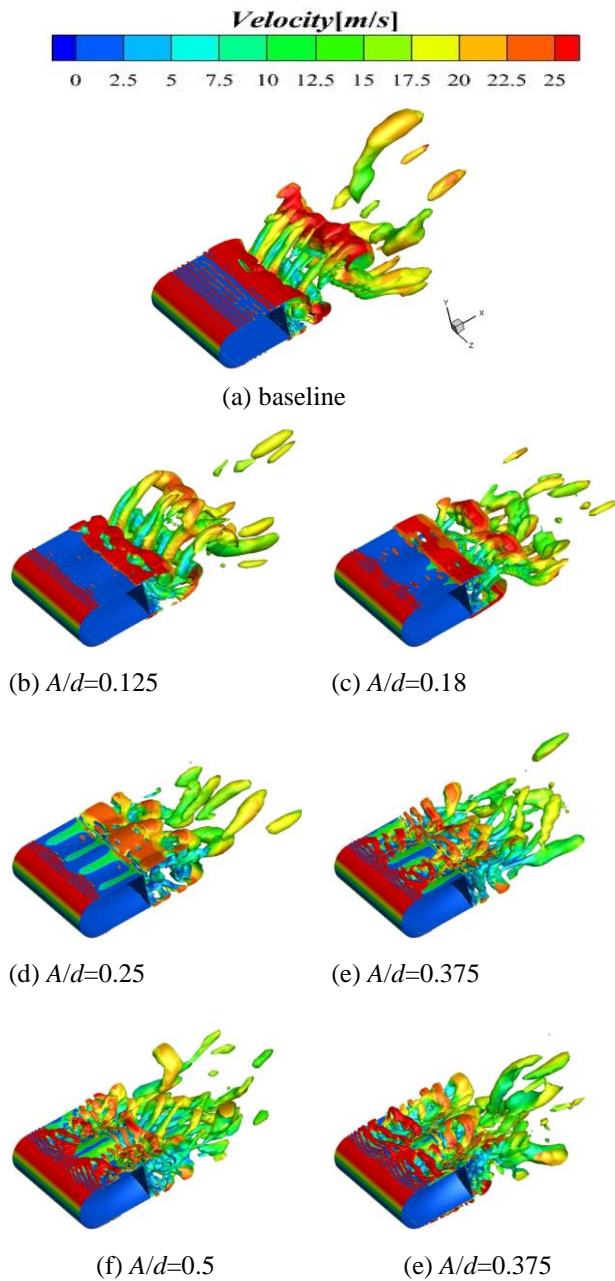


Fig. 10 Comparison of instantaneous vortex structures based on the Q -criterion (non-dimension, $Q=0.5$)

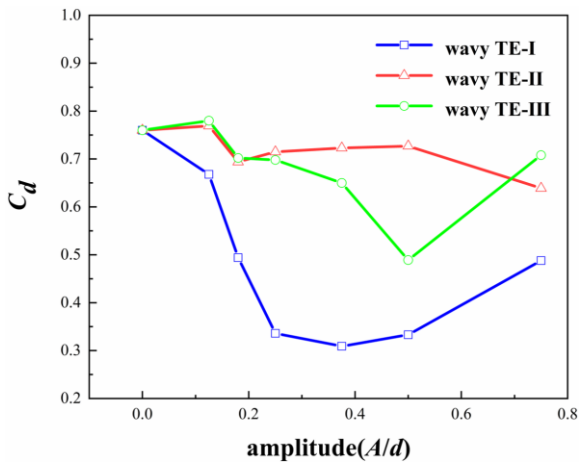


Fig. 11 Comparison of drag coefficients of different wavy TE types

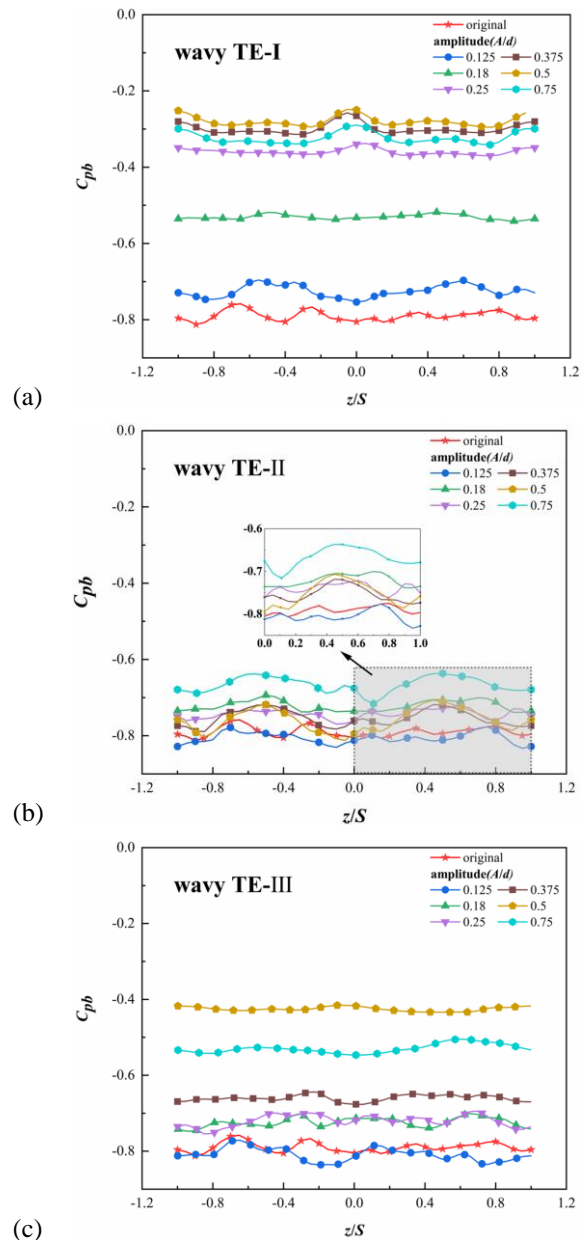


Fig. 12 Comparison of the time-averaged base pressure coefficient

wave types demonstrated significant differences in their influences on the spanwise base pressure coefficients under different wave amplitudes. Compared to the original model, all base pressure coefficient values of the wavy TE-I were higher, particularly at a wave amplitude of $A/d=0.5$, where the base pressure coefficient (\bar{C}_{pb}) escalated to a maximum of -0.280 . This represents a substantial increase of approximately 64.6% compared to the spanwise time-averaged base pressure coefficient of the D-shape, which stands at $\bar{C}_{pb} = -0.790$. Conversely, the overall trend in the variation of the spanwise base pressure coefficient for the wavy TE-III is strikingly similar to that of the wavy TE-I. Despite a slight decrease in the base pressure coefficient, this phenomenon is evident at the minimum designed wave amplitude of $A/d=0.125$, with a value of $\bar{C}_{pb} = -0.809$. This marginal decrease contributes to the slight increase in the drag coefficient observed in the computational results. As for the wavy TE-II, alterations along the

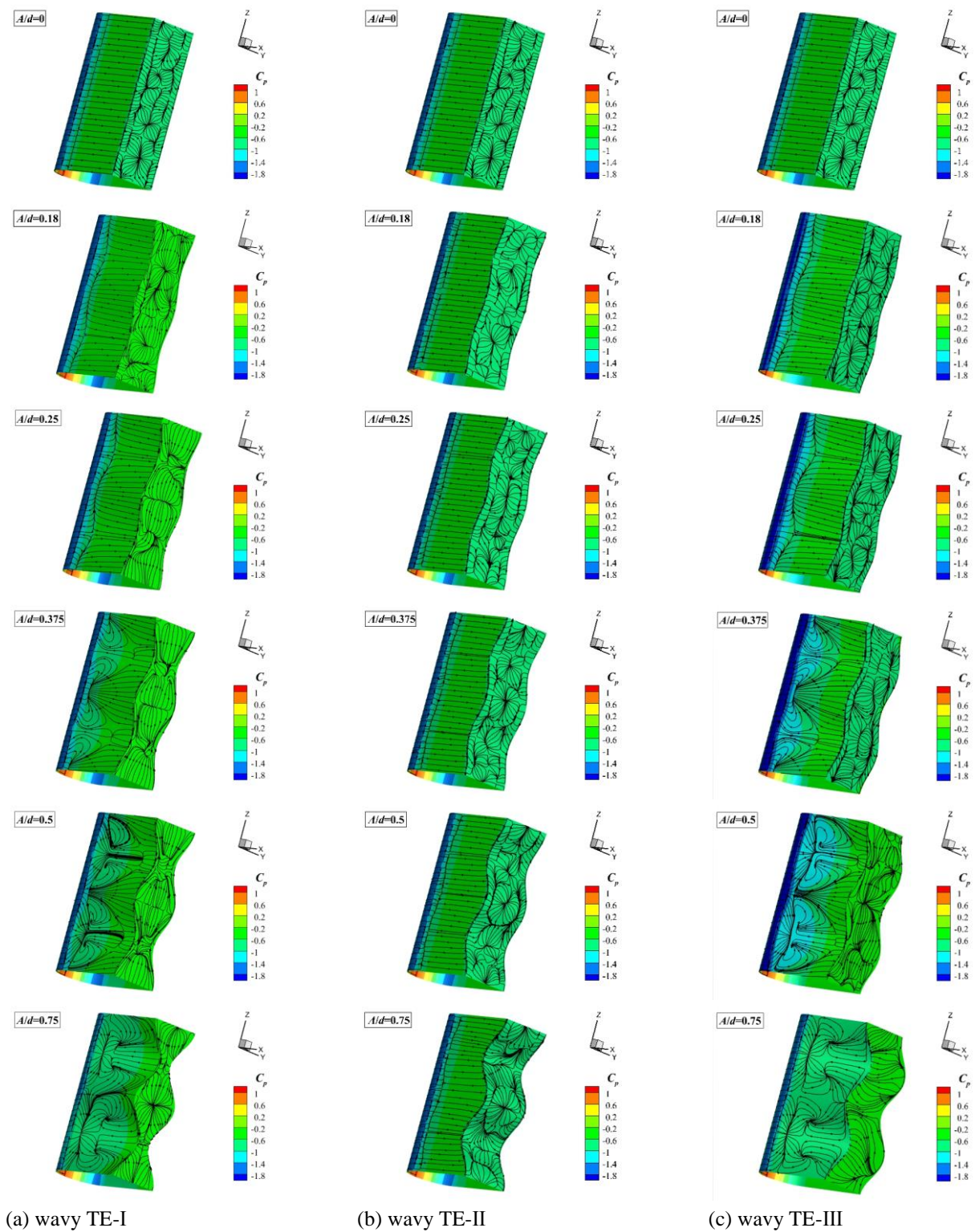


Fig. 13 Comparison of limit streamlines distribution and pressure coefficient contours

spanwise base pressure coefficient remained steady across the various wave amplitudes ($A/d=0.125-0.5$), showing no abrupt surge but still exhibiting some enhancement.

We performed an extensive comparative analysis of the flow-field data to comprehensively elucidate the alterations in the drag and pressure coefficients. Figure 13 depicts the surface-limiting streamlines and pressure-coefficient contour plots for the D-shaped model, along with the three sets of wavy TE and their

corresponding amplitudes. The results indicated that the separation lines of the wave structures varied along the spanwise direction. Owing to the regulatory impact of the wave structures, the surface-limiting streamlines demonstrated a more orderly spanwise distribution than those in the D-shaped model. In the original model, the flow in the front round head area was attached (this area had a lower pressure). As the flow transitioned from the round head to the rectangular area, separation occurred, and the flow separation in

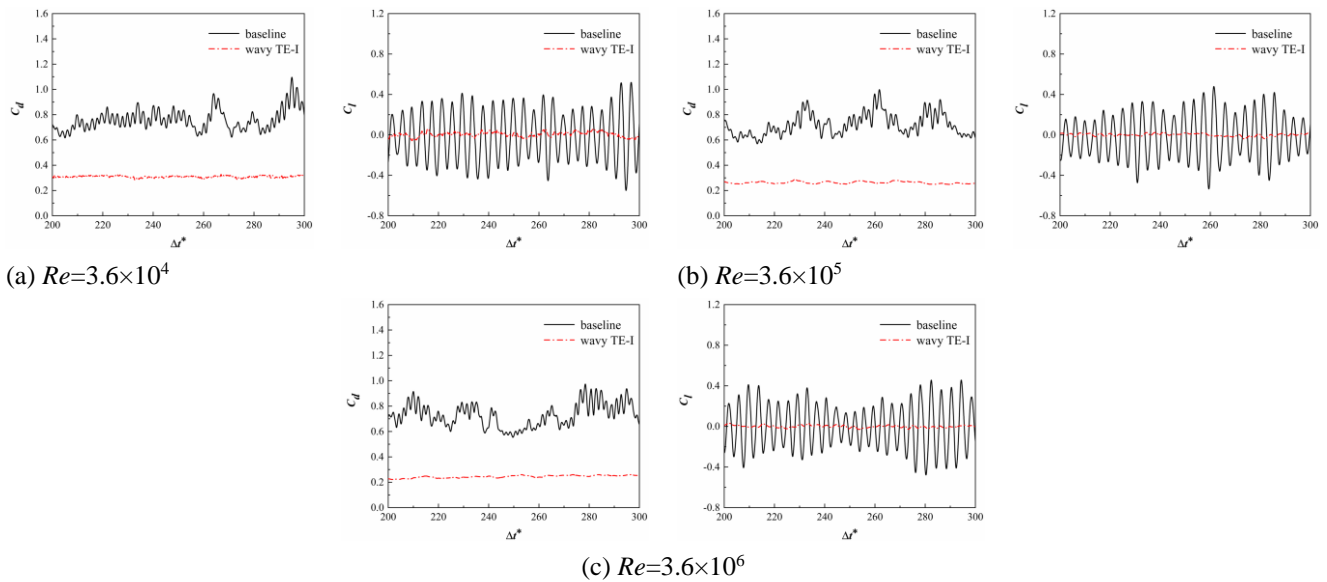


Fig. 14 Time histories of the force coefficients of the D-shaped and wavy TE-I

Table 1 Comparison of main flow quantities

$Re (1 \times 10^4)$	\bar{C}_d		St	
	baseline	wavy TE-I	baseline	wavy TE-I
3.6	0.760	0.309	0.249	...
36	0.719	0.262	0.254	...
360	0.728	0.245	0.262	...

the tail area dispersed to both sides in the spanwise direction. In the modified models, the separation line on the upper surface changed owing to wave perturbations. As the wave amplitude increased, the separation line moved downstream, resulting in a slight decrease in the pressure at that location. Simultaneously, as the wave amplitudes increased, the distribution of the tail-limiting streamlines based on the wave became more regular, and the streamlines converged noticeably towards the troughs at both ends. This convergence was particularly evident in the wavy TE-I and TE-III designs. In contrast, the limiting streamline distribution on the upper surface of wavy TE-II was similar to that of the original D-shaped model. When the wave amplitude was sufficiently large, the flow at the spanwise tail gathered from the raised sides and middle towards the depressed troughs. The negative-pressure area formed at the tail was slightly larger than that in the original D-shaped model, which explains why the spanwise base pressure coefficient exhibited a wavy curve.

3.3 Effect of Reynolds Number

Given the critical guiding role of the Reynolds number in the fluid flow states, and by combining the optimal drag reduction effect of the wave structures mentioned above, we selected wavy TE-I (with specific parameters of wave amplitude $A/d=0.375$ and wavelength $W/D=1.5$) for further exploration. To comprehensively understand its performance, we conducted experimental studies with Reynolds numbers of three different orders of magnitude ($Re=3.6 \times 10^4$, 3.6×10^5 , and 3.6×10^6).

As shown in Fig. 14, the introduction of the wavy structure design significantly altered the tail surface, leading to significant changes in the characteristics of the forces acting on wavy TE-I. In all results, the time-averaged drag coefficient decreased, and the effects became more pronounced as the Reynolds number increased. For Reynolds numbers of different orders of magnitude, the modified average lift coefficients exhibit a similar trend. Compared with the original D-shaped model, the fluctuating lift coefficient of wavy TE-I was suppressed significantly.

Typically, vortex shedding in the wake of a D-shaped model is a significant factor that influences force fluctuations. The detailed flow structures are related to the mean and fluctuating forces, and Strouhal numbers are also closely related to it (Mashhadi et al., 2021). To identify the frequency of wake vortex shedding, the power spectral density (PSD) obtained via the fast Fourier transform (FFT) of the lift coefficient is shown in Fig. 15. Observations revealed that in all the numerical results, the spectral peak of the wavy TE-I model relative to the original model was eliminated, indicating that the periodic vortex shedding in the wake was almost suppressed completely.

To quantitatively analyze the reduction in the mean drag and vortex shedding frequency, Table 1 compares the changes in the time-averaged drag coefficient and Strouhal number owing to the Reynolds number. The results show that the drag coefficients of the original model at high Reynolds numbers are significantly close

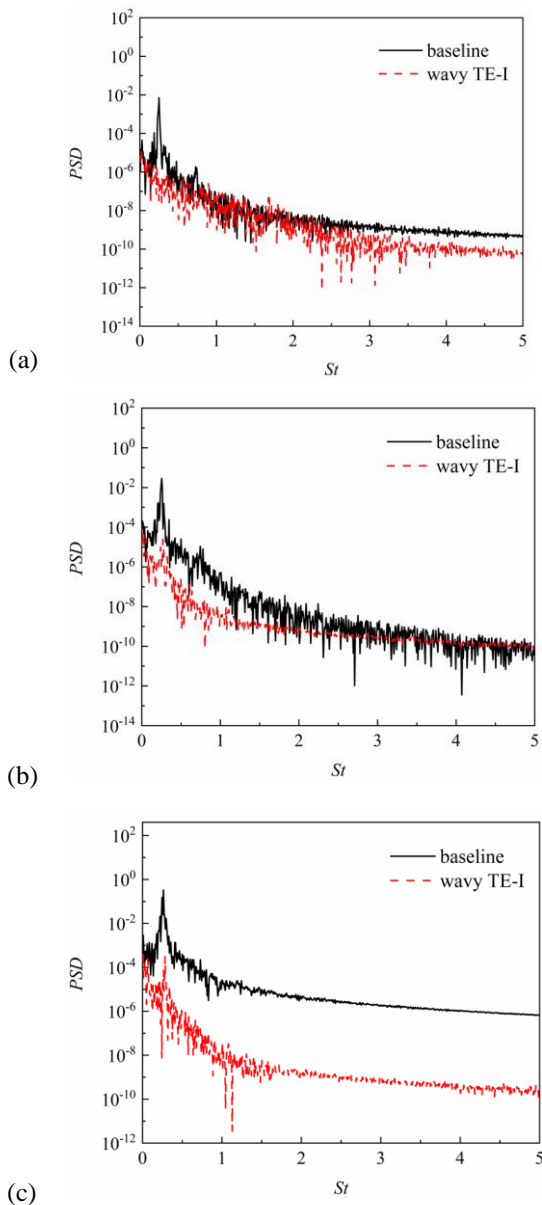


Fig. 15 Comparison of the lift coefficient power spectra of the D-shaped and wavy TE-I. (a) $Re=3.6 \times 10^4$, (b) $Re=3.6 \times 10^5$ and (c) $Re=3.6 \times 10^6$

to each other and smaller compared to those at the $Re=3.6 \times 10^4$ conditions. The drag coefficient values for the wavy TE models are smaller than those of the original model at $Re = 3.6 \times 10^5$ and 3.6×10^6 , with drag reductions of 63.6% and 66.3%, respectively. In addition, the Reynolds number significantly influenced the flow characteristics of a D-shape model with rounded corners (Wang et al., 2024b). As the Reynolds number progressively increased, the Strouhal number associated with vortex shedding also increased in the original model. The typical vortex shedding process of the wavy TE model was suppressed in all three cases such that there were no obvious tonal peaks.

The time-averaged pressure coefficients on the surface of the D-shaped model are compared in Fig. 16. All calculation results indicated similar changes in the pressure coefficient distribution across the entire upper surface. The pressure coefficients at the three cross-sections of the wave modification on the front

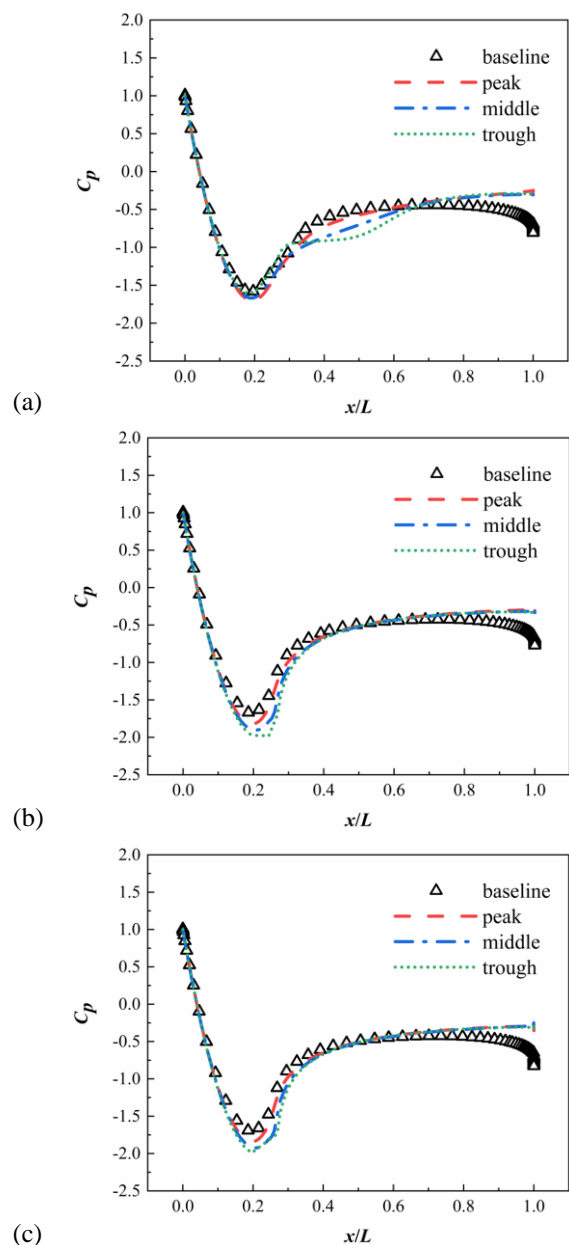


Fig. 16 Time-averaged pressure coefficient distribution on the surface of the D-shaped and wavy TE-I. (a) $Re=3.6 \times 10^4$, (b) $Re=3.6 \times 10^5$ and (c) $Re=3.6 \times 10^6$

round head were all lower than those of the original model, with the maximum pressure coefficient values obtained in the downstream tail region. Notably, under the smallest Reynolds number condition ($Re=3.6 \times 10^4$), the increase in the pressure coefficient in the central region where the round head transitioned to the flat back showed a sharper rise, followed by a steady recovery. In contrast, under the influence of the two higher Reynolds numbers, the recovery of the pressure coefficient in the transition region remained smooth. Overall, the increase in the pressure coefficient caused by the wavy structural design is an important reason for the effective reduction in the drag coefficient.

As shown in Fig. 17, the incoming time-averaged velocity (nondimensional) along the wake centerline ($y=0$) of the wavy TE was compared with that of the D-shaped model. The trends in the wake streamline

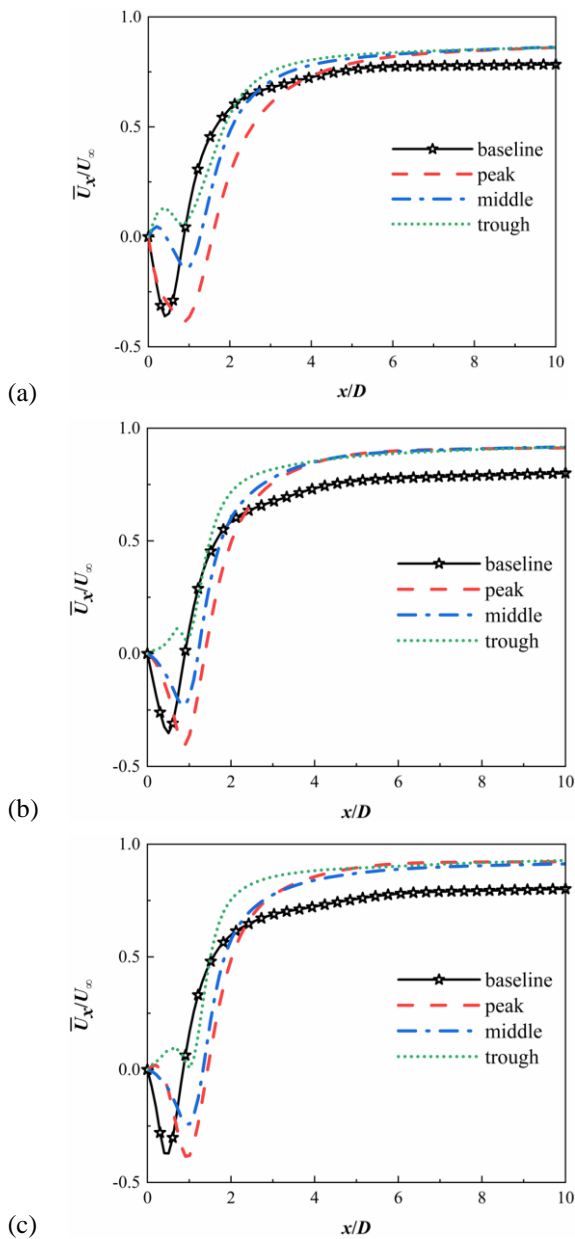


Fig. 17 Mean stream velocity distribution along the central line at $y=0$ of the D-shaped and wavy TE-I. (a) $Re=3.6\times 10^4$, (b) $Re=3.6\times 10^5$ and (c) $Re=3.6\times 10^6$

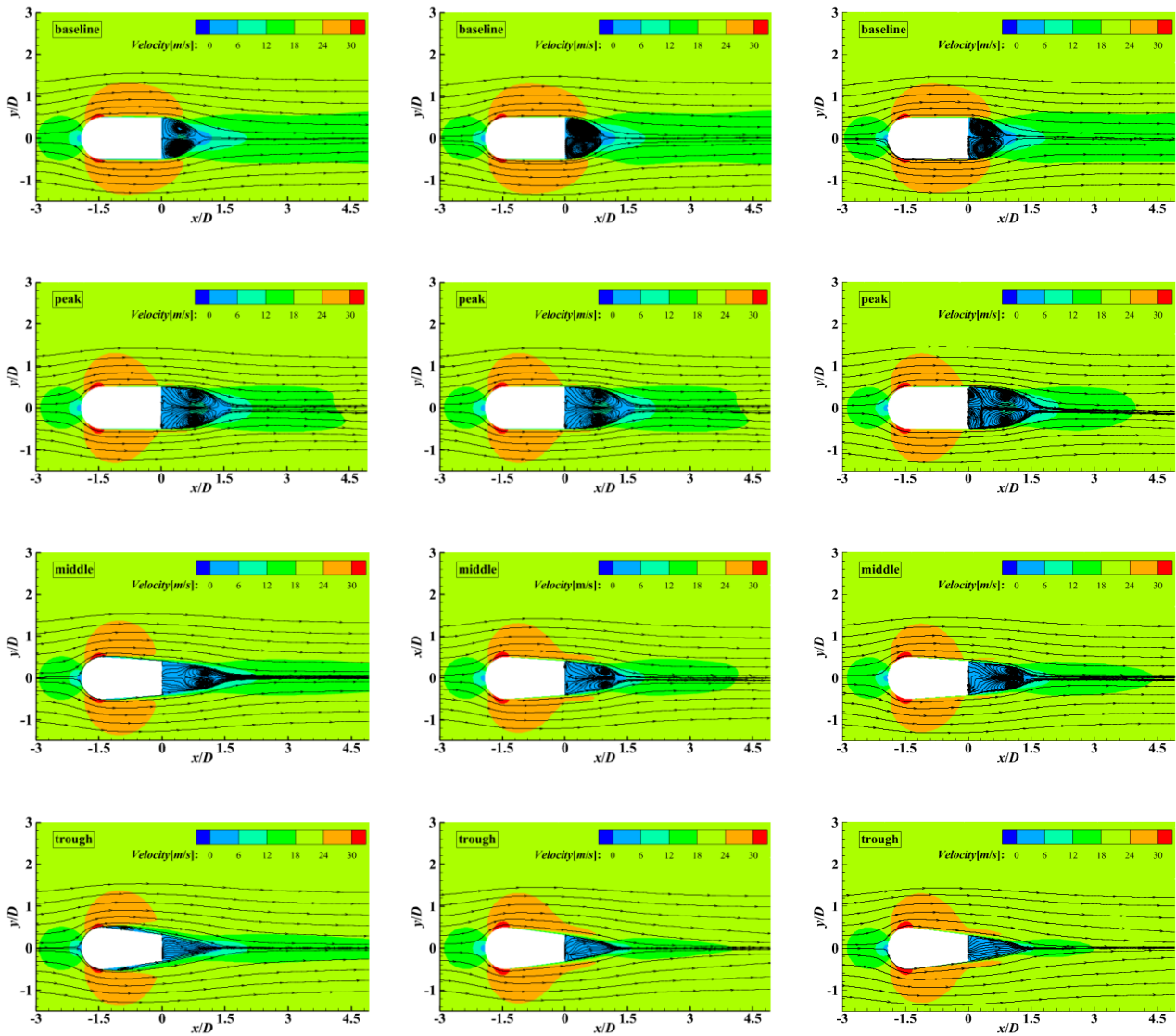
distribution were consistent across all the calculated cases and their corresponding baselines. In the tail region of the D-shaped model, owing to vortex shedding on the surface, the time-averaged flow velocity decreased with the development of the flow. The time-averaged flow velocity reached its minimum value in the turbulent core region and recovered as the downstream flow continued to develop, eventually maintaining the same level as that of the upstream time-averaged velocity. However, the velocity distribution of the wake region at different cross-sections of the wavy TE-I model exhibited some changes. The position of the minimum velocity was delayed, moving downstream. Compared to the baseline trend of the original model, the wavy structure significantly altered the flow structures of the tail, placing the turbulent core region further downstream in the wake. Additionally, the negative flow velocities under

the three sets of Reynolds numbers were significantly reduced, and there was no negative flow velocity at the centerline of the wave trough cross section, indicating that wavy TE-I had a certain inhibitory effect on the backflow in the wake region under different Reynolds number conditions. These findings provide an important theoretical basis for further understanding and optimizing the design of passive control methods for aerodynamic drag.

To ensure consistent non-dimensional time steps, Fig. 18 illustrates a comparison of the mean velocity magnitude distribution contours and time-averaged streamwise velocity streamlines. In all the cases, the wavy structure destabilized the shear layer, and this instability primarily occurred in the upstream region close to the front. On the peak and middle cross-sections, the wake region maintained a symmetrical primary vortex structure similar to that of the original model, but its size was larger, and the turbulent core region shifted downstream. This resulted in an increased pressure and flow velocity near the tail region. For the trough plane, the flow in the wake region appeared relatively stable, and the periodic vortex structure ceased to exist. In addition, the tailvortex that interfered with the front flow of the main body was suppressed, and this was a crucial reason for the absence of negative values in the time-averaged incoming flow velocity on its cross section. Overall, the wavy TE design enhanced the instability characteristics of the shear layer by altering the flow structures, and to some extent, suppressed the shedding of the separation vortices at the tail.

Figure 19 compares the surface-limiting streamlines and pressure coefficient contours of the D-shaped and wavy TE-I models under three sets of Reynolds numbers. At a Reynolds number of $Re=3.6\times 10^4$, there exist an attached flow and recirculation in the transition region of the models. The wavy TE interfered with the flow structures on the upper surface, and a recirculation convection occurred near the end of the front round head at $x/L=0.026$. Meanwhile, the low-pressure region expanded slightly owing to wave perturbation. Compared with the original model, the limiting streamlines on the back of the wavy TE-I model were more regularly distributed, moving laterally along the spanwise direction and intersecting at the cross section of the trough. As the Reynolds numbers increases to $Re=3.6\times 10^5$ and 3.6×10^6 , the flow field structures exhibited similar flow states, resulting in a more regular spanwise distribution on the back of wavy TE-I. However, owing to the influence of the increased Reynolds number and boundary layer effects, the attached flow covered the entire upper surface of both the D-shaped and wavy TE-I models, eliminating any signs of backflow.

To provide a clearer understanding of the influence of the tail modifications on the flow structures across varying Reynolds numbers, the iso-surface of the Q -criterion (non-dimensional, $Q=0.5$) was employed to visualize the flow field traits of both the D-shaped and wavy TE-I configurations, as depicted in Fig. 20. Under the three different flow conditions, the separated shear layer on the upper surface of the unmodified D-shaped model became unstable downstream, and this was accompanied by pronounced large-scale vortex patterns behind the tail. In contrast, the wavy structure maintained



(a) $Re=3.6 \times 10^4$ (b) $Re=3.6 \times 10^5$ (c) $Re=3.6 \times 10^6$

Fig. 18 Mean streamlines and mean velocity magnitude contours on cross-sections

its original shear layer properties at its front but experienced disruption and heightened instability in the tail area. Consequently, the large vortex structures disintegrated into smaller ones and became densely packed in the tail region. As the Reynolds number increased, the disruptive effect of the original D-shaped tail flow on the front segment diminished, leading to the disappearance of the unstable shear layer within the primary rectangular zone. Furthermore, the accumulation of the scattered small vortex structures in the frontal depression area was suppressed as the Reynolds numbers increased, owing to the interference from the tail flow field. Overall, the introduction of the wavy TE significantly reduced the vortex scale and effectively suppressed the shedding of periodic vortices, thereby favorably enhancing the flow field structures.

4. CONCLUSIONS

By employing the IDDES numerical simulation method, this study investigated the aerodynamic

performance and flow field of a D-shaped bluff body with a wavy TE. The study encompassed variations in five wavelengths, seven amplitude sets, three distinct types of wavy TE structures, and three different flow regimes within the Reynolds number range of 3.6×10^4 to 3.6×10^6 . Through meticulous observation of vortex formation and evolution, a thorough analysis was conducted on the underlying control mechanism of wavy structures and their attendant physical implications. The conclusions are as follows:

- (1) The pressure distribution in the base region of a D-shape with a wavy TE is closely related to its force. Because of the higher pressure distribution in the base region of the wavy TE design, the average drag coefficient can be reduced. Specifically, based on the wavy TE-I configuration, the improved aerodynamic performance was highly sensitive to amplitude variations. More precisely, when the amplitude was set to 0.375, the average base pressure coefficient along the spanwise direction significantly increased by approximately 62.1%, and the drag coefficient decreased to approximately

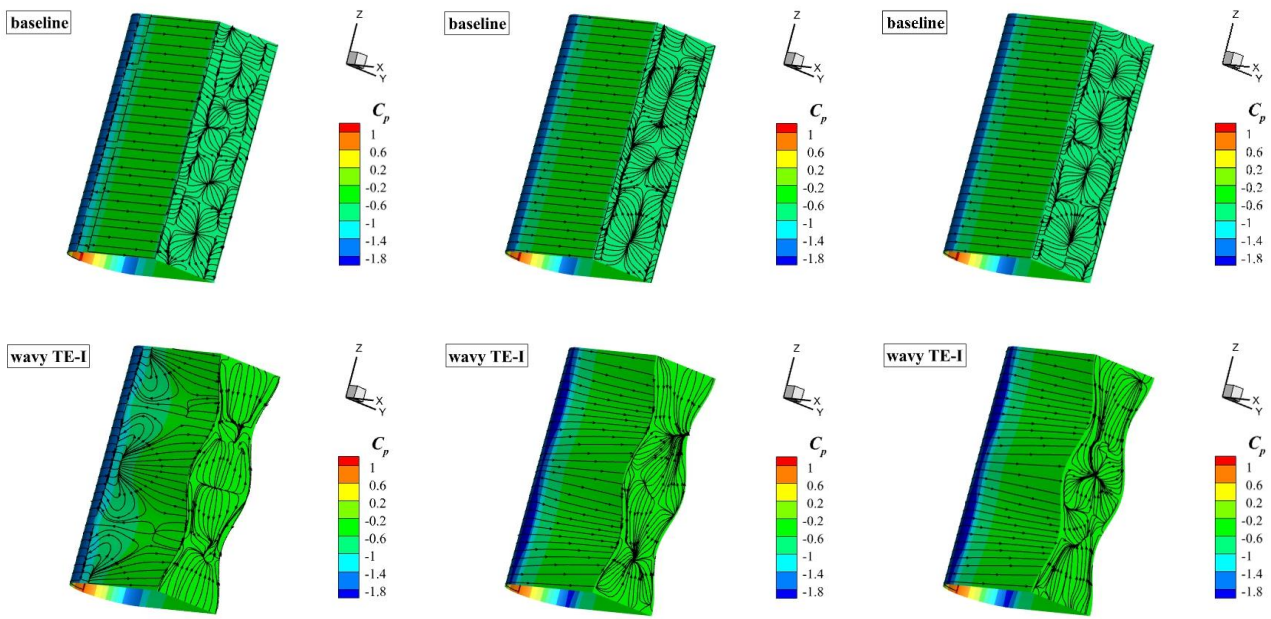


Fig. 19 Comparison of the surface limiting streamlines with pressure coefficient contour on the D-shaped and wavy TE-I

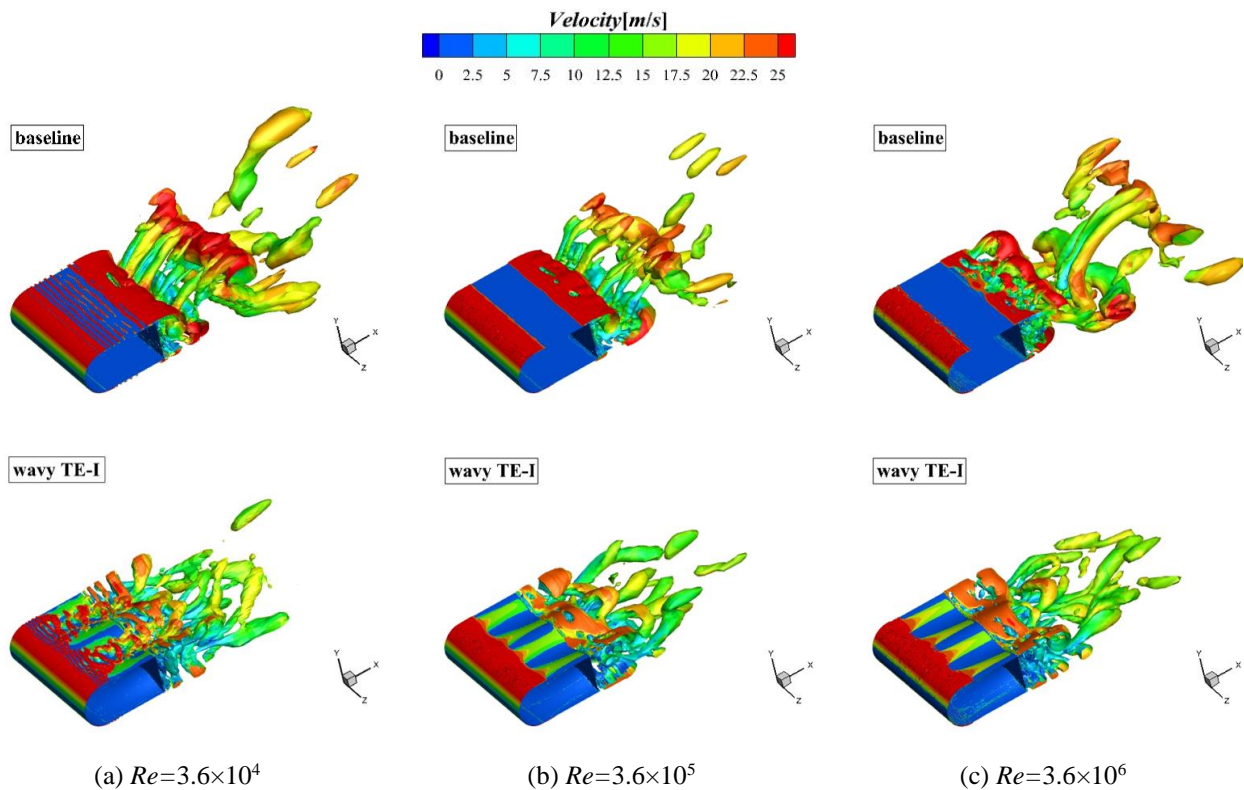


Fig. 20 Comparison of instantaneous vortex structures by the iso-surface of the Q -criterion (non-dimension, $Q=0.5$)

0.310. Compared with the original D-shaped bluff body, the modified design achieved a drag reduction of up to 60.2%. Although wavelength is a variable parameter, it did not exhibit a strong influence in this study. We hypothesized that this may be due to the insufficient range of wavelengths selected in the study to induce significant changes in the internal flow. Therefore,

the influence of wavelength on aerodynamic performance remains a variable requiring of further investigation.

(2) Compared to the other two wavy structures, the wavy TE-I structure demonstrated a more significant drag reduction effect. This was primarily attributed to the strong perturbation of the boundary layer caused by the

wavy geometry. Such perturbations led to a significant disruption of the separated shear layer on the main body surface, thereby enhancing the instability characteristics of the shear layer. Additionally, the vortices located on the surface of the wavy TE-I structure tend to be more concentrated in the concave regions, and the vortex structures at the tail evolved from large-scale to smaller eddy structures.

(3) Under three different flow conditions, the bottom area of the wavy TE structure exhibited a higher base pressure coefficient distribution. Simultaneously, the average drag coefficient decreased, and the fluctuation of the lift coefficient was suppressed. This phenomenon is attributed to the instability of the downstream shear layer caused by the wavy structure, which leads to changes in the position of the turbulent core region. Specifically, under the Reynolds numbers of 3.6×10^5 and 3.6×10^6 , the original quasi-symmetric vortex structure on the cross-section of the trough completely disappeared, and there is no longer any backflow phenomenon. Therefore, based on the significant effects demonstrated by this passive control method, the pivotal role of the wavy TE structure in drag reduction was further verified. The underlying flow-control mechanism has tremendous research value and deserves further in-depth exploration.

ACKNOWLEDGEMENTS

This work is supported by the National Nature Science Foundation of China (Grant No. 52476213).

CONFLICT OF INTEREST

The authors have no conflict interests to disclose.

AUTHORS CONTRIBUTION

Haojie Yang: Investigation, Writing - Original Draft;
Dahai Luo: Supervision, Writing - Review & Editing;
Tao Wang: Investigation, Resources.

REFERENCES

- Bearman, P. W., & Tombazis, N. (1993). The Effects of three-dimensional imposed disturbances on bluff body near wake flows. *Journal of Wind Engineering and Industrial Aerodynamics*, 49, 339-349
[https://doi.org/10.1016/0167-6105\(93\)90029-n](https://doi.org/10.1016/0167-6105(93)90029-n)
- Bearman, P., & Owen, J. C. (1998). Reduction of bluff body drag and suppression of vortex shedding by the introduction of wavy separation lines. *Journal of Fluids and Structures*, 12, 123-130.
<https://doi.org/10.1006/jfls.1997.0128>.
- Chen, B., Yang, X., Chen, G., Tang, X., Ding, J., & Weng, P. J. P. O. F. (2022). Numerical study on the flow and noise control mechanism of wavy cylinder. *Physics of Fluids*, 34, 036108.
<https://doi.org/10.1063/5.0082896>
- Chen, J. L., & Liao, Y. H. (2021). Effects of an annular plasma actuator on a co-flow jet downstream of a bluff-body. *Applied Thermal Engineering*, 192, 116975.

- <https://doi.org/10.1016/j.applthermaleng.2021.116975>
- Chen, W., Qiao, W., & Wei, Z. (2020). Aerodynamic performance and wake development of airfoils with wavy leading edges. *Aerospace Science and Technology*, 106, 106216.
<https://doi.org/10.1016/j.ast.2020.106216>
- Dai, Q. Qi, E., Huang, S., Zhou, Z., & Wang, Y. (2024). Research on active flow control method of NACA0012 airfoil with traveling wave structure. *Journal of Applied Fluid Mechanics*, 17(6), 1293-1305. <https://doi.org/10.47176/jafm.17.6.2301>
- Darekar, R., & Sherwin, S. (2001). Flow past a bluff body with a wavy stagnation face. *Fluids Structures*, 15, 587-596. <https://doi.org/10.1006/jfls.2000.0354>
- Fish, F. E., & Battle, J. M. (1995). Hydrodynamic design of the humpback whale flipper. *Journal of Morphology*, 225, 51-60.
<https://doi.org/10.1002/jmor.1052250105>
- Kourta, A., & Leclerc, C. (2013). Characterization of synthetic jet actuation with application to Ahmed body wake. *Sensors Actuators A: Physical* 192, 13-26. <https://doi.org/10.1016/j.sna.2012.12.008>
- Krishan, G., Oo, N. L., & Sharma, R. N. (2023). Flow-field characteristics of a synthetic jet impinging on a circular cylinder in a free and constrained environment. *European Journal of Mechanics - B/Fluids* 99, 116-135.
<https://doi.org/10.1016/j.euromechflu.2023.01.009>
- Marec, J. P. (2001). *Drag reduction: a major task for research*. Aerodynamic Drag Reduction Technologies: Proceedings of the CEAS/ DragNet European Drag Reduction Conference, 19-21 June 2000, Potsdam, Germany. Springer, pp. 17-27.
https://doi.org/10.1007/978-3-540-45359-8_3
- Mashhadi, A., Sohankar, A., Alam, M. M. (2021). Flow over rectangular cylinder: Effects of cylinder aspect ratio and Reynolds number. *International Journal of Mechanical Sciences*, 195, 106264.
<https://doi.org/10.1016/j.ijmecsci.2020.106264>
- Post, M. L., & Corke, T. C. (2004). Separation control on high angle of attack airfoil using plasma actuators. *AIAA Journal* 42, 2177-2184.
<https://doi.org/10.2514/1.2929>
- Qi, W. C., Cheng, K., Li, P. C., & Li, J. Y. (2024). Enhancing axial fan noise reduction through innovative wavy blade configurations. *Journal of Applied Fluid Mechanics*, 17(7), 1430-1443.
<https://doi.org/10.47176/jafm.17.7.2442>
- Shi, L., Wang, Y., Zhang, G., Jin, Y., & Zhang, D. (2020). Assessment of an improved turbulence model in simulating the unsteady flows around a D-shaped cylinder and an open cavity. *Applied Mathematical Modelling* 83, 552-575.
<https://doi.org/10.1016/j.apm.2020.01.068>
- Shi, Y., & Kollmann, W. (2021). Improved delayed detached eddy simulation of a porous wavy trailing edge. *Physics of Fluids*, 33, 055128.
<https://doi.org/10.1063/5.0050261>

- Smith, T., & Klettner, C. (2022). Airfoil trailing-edge noise and drag reduction at a moderate Reynolds number using wavy geometries. *Physics of Fluids*, 34, 117107. <https://doi.org/10.1063/5.0120124>
- Thiria, B., Cadot, O., & Beaudoin, J. F. (2009). Passive drag control of a blunt trailing edge cylinder. *Journal of Fluids and Structures* 25, 766-776. <https://doi.org/10.1016/j.jfluidstructs.2008.07.008>
- Tombazis, N., & Bearman, P. (1997). A study of three-dimensional aspects of vortex shedding from a bluff body with a mild geometric disturbance. *Journal of Fluid Mechanics* 330, 85-112. <https://doi.org/10.1017/S0022112096003631>
- Wang, K., Liu, L., Huang, H. X., Tan, H. J., Tang, X. B., & Zheng, G. J. (2024a). Behavior of flow distortion within a boundary layer ingestion inlet. *Aerospace Science and Technology* 146, 108947. <https://doi.org/10.1016/j.ast.2024.108947>
- Wang, R., Zuo, X., He, Y., Pi, W., Zhu, Y., Wu, C., & Wei, Y. (2024b). Numerical study of the effects of aspect ratio and Reynolds number on the flow over a rectangular cylinder with rounded corners. *Ocean Engineering*, 297, 117115. <https://doi.org/10.1016/j.oceaneng.2024.117115>
- Xing, Y., Chen, W., Wang, X., Tong, Fan., & Qiao, W. (2023). Effect of wavy leading edges on airfoil trailing-edge bluntness noise. *Aerospace*, 10(4), 353. <https://doi.org/10.3390/aerospace10040353>
- Xu, W., Li, C. C., Huang, S. X., & Wang, Y. (2022). Aerodynamic performance improvement analysis of savonius vertical axis wind turbine utilizing plasma excitation flow control. *Energy*, 239, 122133. <https://doi.org/10.1016/j.energy.2021.122133>
- Yang, S. J., & Baeder, J. D. (2019). Aerodynamic and aeroacoustic behavior of span-wise wavy trailing edge modified SNL 100 m blade. *Wind Engineering* 43, 4-25. <https://doi.org/10.1177/0309524X18818646>
- Yang, S., & Baeder, J. (2016). *Effect of wavy trailing edge on 100meter flatback wind turbine blade*. Journal of Physics: Conference Series. IOP Publishing, p. 022060. <https://doi.org/10.1088/1742-6596/753/2/022060>
- Zhang, M., Wang, G., & Xu, J. (2013). *Effect of humpback whale-like leading-edge protuberances on the low Reynolds number airfoil aerodynamics*. Fluid-Structure-Sound Interactions and Control: Proceedings of the 2nd Symposium on Fluid-Structure-Sound Interactions and Control. Springer, pp. 107-113. https://doi.org/10.1007/978-3-642-40371-2_1